Physics – Uspekhi **59** (5) 487 – 501 (2016)

CONFERENCES AND SYMPOSIA

PACS numbers: 42.25.Dd, 42.62.Be, 43.35.Sx, **87.64.–t**, 87.64.Cc

Methods of biomedical optical imaging: from subcellular structures to tissues and organs

I V Turchin

DOI: 10.3367/UFNe.2015.12.037734

Contents

1. Introduction **487**

2. Fluorescence microscopy **489**

2.1 Multiphoton microscopy; 2.2 Nanoscopy; 2.3 Optical projection tomography and light-sheet fluorescence microscopy

3. Optical coherence tomography **491**

3.1 Clinical applications of optical coherence tomography; 3.2 High-frequency optical coherence tomography and analysis of speckle structure; 3.3 Spectroscopic optical coherence tomography; 3.4 Optical coherence microscopy; 3.5 Contrast enhancement in optical coherence tomography; 3.6 Automatic detection of diseases by analyzing optical coherence tomography images

4. Optoacoustics **493**

4.1 Imaging depth in optoacoustics; 4.2 Spatial resolution in optoacoustics; 4.3 Chromophore separation in optoacoustics; 4.4 Optoacoustic microscopy and tomography; 4.5 Biomedical applications of optoacoustics

5. Diffuse optical spectroscopy and tomography **495**

5.1 General information on diffuse optical spectroscopy; 5.2 Continuous wave, time-domain, and frequency-domain approaches in optical diffuse spectroscopy; 5.3 General information on diffuse optical tomography; 5.4 Boundary conditions in diffuse optical tomography; 5.5 Solution of the inverse problem of diffuse optical tomography; 5.6 Other diffuse optical methods for the study of biological tissues

6. Macroscopic fluorescence imaging techniques **497**

6.1 Surface fluorescence imaging techniques for the study of biological tissues; 6.2 Fluorescence tomography; 6.3 Fluorescence projection methods for the study of biological tissues; 6.4 Spectral and time-resolved separation of fluorophores; 6.5 Fluorescent markers; 6.6 Near-infrared fluorescence imaging

7. Conclusion **499**

References **500**

Abstract. Optical bioimaging methods have a wide range of applications in the life sciences, most notably including the molecular resolution study of subcellular structures, small animal molecular imaging, and structural and functional clinical diagnostics of tissue layers and organs. We review fluorescent microscopy, fluorescent macroscopy, optical coherence tomography, optoacoustic tomography, and optical diffuse spectroscopy and tomography from the standpoint of physical fundamentals, applications, and progress.

Keywords: optical bioimaging, biophotonics, optical coherence tomography, fluorescent microscopy, optical nanoscopy, optoacoustics, optical diffusion tomography, fluorescent agents, fluorescent proteins, upconversion nanoparticles, STED, STORM

I V Turchin Institute of Applied Physics, Russian Academy of Sciences, ul. Ul'yanova 46, 603950 Nizhny Novgorod, Russian Federation
Tel. +7 (831) 436 80 10
E-mail: ilya@ufp.appl.sci-nnov.ru

Received 22 January 2016
Uspekhi Fizicheskikh Nauk **186** (5) 550–567 (2016)
DOI: 10.3367/UFNr.2015.12.037734
Translated by Yu V Morozov; edited by A M Semikhatov

1. Introduction

As a light beam propagates in biological tissues, photons are scattered by microinhomogeneities of the dielectric permittivity and absorbed by endogenous and exogenous chromophores [1]. Photon absorption by tissue chromophores gives rise to a variety of physical events, e.g., heat release leading to local thermoelastic expansion of the tissue responsible for the generation of an optoacoustic wave. There are also biological structures exhibiting intrinsic fluorescence and emitting long-wavelength photons when absorbing light (Stokes shift). High-intensity radiation can induce multiphoton fluorescence in which coherent absorption of several photons at a time results in the emission of a single photon with the wavelength shorter than that of the exciting radiation. A change in the wavelength of the probing radiation can also be a consequence of inelastic (Raman) scattering of light. Elastic scattering produces effects such as beam smearing, backscattering, and polarization.

Each of these physical events can be used as a contrast agent to form images of the internal structure of a biotissue.

Table 1. Optical methods for the study of biological tissues with the respective limiting imaging depths and spatial resolution.

Method	Contrast	Imaging depth	Resolution*
Microscopy	Fluorescence brightness	1 μm	10 nm
		200 μm	3(0.3) μm
		1 mm	6 μm
Optical coherence tomography	Backscattering coefficient, degree of depolarization	0.4 mm	1 μm
		2 mm	10 μm
Optoacoustic visualization	Absorption coefficient	3 mm	15(45) μm
		5 cm	700 μm
Diffuse optical methods	Refractive index and reduced scattering coefficient	10 cm	1 cm
Microscopic fluorescence methods	Fluorescence brightness	10 cm	1 cm

* Figures outside parentheses refer to longitudinal resolution; those inside refer to transverse resolution.

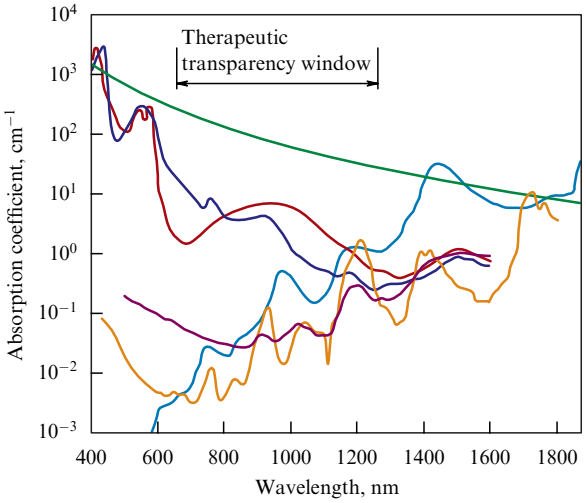

Figure 1. (Color online.) Absorption spectra of endogenous chromophores. Red and dark-blue lines are oxy- and desoxyhemoglobins, respectively (150 g l^{-1}) [3]; light-blue — water, brown — lipids, green — melanin [4], violet — collagen [5, 6].

Table 1 lists optical methods for the study of biological tissues and presents data on their limiting imaging depths, spatial resolution, and optical contrast with which an image is formed. Each method is based on probing the tissue with a probing beam and detecting scattered light, fluorescence, or an acoustic wave.

The imaging depth and spatial resolution are limited by absorption and scattering, with the biotissue scattering coefficient exhibiting a smooth dependence on the wavelength, and the absorption coefficient being a more complex quantity, as shown in Fig. 1 [2]. In the wavelength range 600–1300 nm, known as the therapeutic transparency window, absorption by biological tissues is relatively low and becomes even lower in the narrow range 700–900 nm, where most studies are carried out at a maximum depth of 10 cm. The light penetration depth in tissues closer to the short-wavelength part (violet and ultraviolet end) of the optical spectrum is limited by strong melanin and blood absorption. Water is the main chromophore limiting the application of optical methods for deep imaging in the long-wavelength part of the spectrum.

The spatial resolution of optical methods drops with depth due to strong light scattering responsible for the smearing of the illumination beam. Different light propagation regimes are realized at different depths.

At a depth less than 1–2 photon mean free paths, the probing beam propagates without scattering, which permits achieving the limit optical resolution equivalent to the diffraction limit. It is in this narrow surface layer ($\sim 100-200$ μm) that light microscopy studies are carried out. In Section 2, we also discuss nanoscopic techniques whose spatial resolution exceeds the diffraction limit; these methods are applicable in an even narrower layer of about 1 μm.

At greater depths, the probing beam broadens due to scattering, with small-angle scattering prevailing over the large-angle one by virtue of the specificity of the scattering indicatrix. The beam retains its structure at depths up to 1–2 photon transport lengths ($\sim 1-2$ mm). So-called coherence techniques were shown to be especially suitable for studying biotissues within this depth range, e.g., optical coherence tomography (OCT) in which photons backscattered by the tissue are detected in a time-resolved mode (see Section 3).

At depths of several photon transport lengths, light becomes diffuse, i.e., photons completely 'forget' their initial propagation direction. Evidently, it is very difficult to achieve an acceptable spatial resolution at such depths by purely optical methods.

The problem of diffuse optical tomography (DOT) is ill-posed, and solving it requires knowing the shape of the study object, using a large number of projections obtained with high signal-to-noise ratio, and relying on intricate iterative algorithms essentially different from those used in X-ray tomography. High spatial resolution at large depths (over 1–2 photon transport lengths) can be achieved only by a combination of optical and other (ultrasound, magnetic resonance, X-ray) methods in which scattering does not actually interfere with image formation. For example, optoacoustic (OA) visualization techniques with ultrasound location of light-absorbing chromophores have recently found wide application.

Describing light propagation processes in biological tissues is of primary importance for the identification of physical limitations of imaging techniques, their design, and elaboration of algorithms for reconstructing the internal structure of the tissue. In most cases, except manifestations of coherence effects, light propagation in biological tissues is fairly well described by the radiative transfer equation (RTE) [7]. In general, the RTE is an integro-differential equation having no analytic solution. Therefore, its various approximations (Bouguer–Lambert–Beer law, small-angle and diffusion approximations) proposed earlier in underwater and atmospheric imaging theory are typically used to address problems pertaining to optical visualization of biological tissues. Currently, Monte Carlo (MC) simulation is considered to be the most efficient numerical method for the statistical modeling of photon trajectories in scattering and absorbing media. Recently, the developers of MC codes have managed to significantly shorten the optical field calculation time by using multiprocessors, such as a graphic processor

unit (GPU) with more than 1000 cores [8], rather than by increasing the processor speed (which has not changed much in the past several years).

An optical image can form on scattering, absorption, and fluorescence brightness variations characterizing functional and structural properties of biological tissues. The high contrast of these parameters is a distinctive feature of optical imaging methods, in comparison with X-ray and ultrasound. For example, malignant neoplasms are characterized by an abnormally high scattering coefficient due to an increased nuclear–cytoplasmic ratio. The main tissue chromophores (oxy- and desoxyhemoglobins, water, lipids, melanin, collagen) serving as indicators of the functional state of biological tissues have different absorption coefficients, which allows the component composition to be reconstructed by optical spectroscopic techniques.

We note that assessing the absorption coefficient in a biotissue requires that the probing light cover a rather long distance because the absorption coefficient is much smaller than the scattering coefficient in the transparency window. This means that light must undergo multiple scatterings before information about absorbed photons appears in the beam. For this reason, biotissue spectroscopy is performed by diffuse optical methods, described in Section 5.

In microscopy, where the imaging depth does not exceed 1–2 photon mean free paths, the component composition can be reconstructed either by Raman spectroscopy [9] or by fluorescence visualization, i.e., upon a change in the wavelength of radiation being measured relative to the probing radiation wavelength.

The highest contrast in biotissue visualization can be reached by using fluorescence methods, because spectral bands of probing and recorded radiation are easy to separate by optical filters. There are many bright exogenous markers besides endogenous fluorescent molecules, e.g., fluorescent proteins (FPs), organic dyes, and synthetic nanoscale agents that can be specifically bound to the biological structures of interest. Such specific labeling can be referred to as molecular imaging, comparable only to positron emission tomography (PET) in terms of sensitivity (Fig. 2).

Optical visualization methods for biological tissues are applied in a variety of biomedical research at different scales, such as subcellular, cellular, tissue, and organismic levels in small laboratory animals and human organs (breast, muscles, brain). The optical methods for such investigations, their physical basis, advantages, and disadvantages are described in Sections 2–6. Fluorescence imaging techniques for biological tissues are subdivided into microscopic (Section 2) and macroscopic (Section 6), depending on the maximum attainable imaging depth: below 1–2 photon mean free paths in microscopy and above that in macroscopic methods.

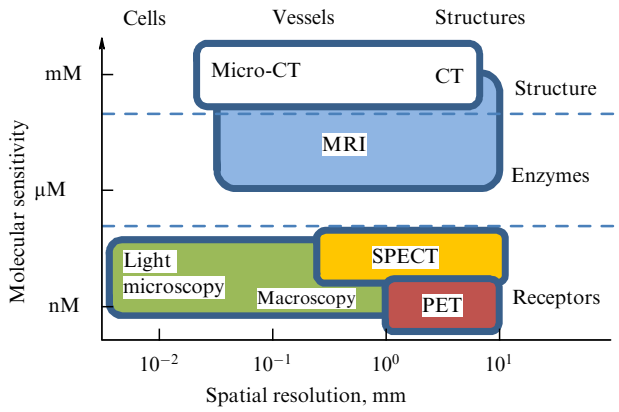

Figure 2. Comparison of molecular sensitivity of various visualization techniques: CT — computed tomography, MRI — magnetic resonance imaging, SPECT — single photon emission computed tomography. Cellular and subcellular resolutions in optical microscopy are attainable only at small depths.

2. Fluorescence microscopy

It was noted in Section 1 that optical imaging methods for visualization in narrow layers as thick as 1–2 photon mean free paths do not yield information about scattering and absorbing properties of an object. Phase contrast microscopy using the refractive index discontinuity as a contrast allows only the contours of a biological object to be seen, i.e., provides very poor information. Therefore, microscopy mostly uses methods in which probing and recorded radiation has different wavelengths, as in Raman and fluorescence microscopy.

The main lines of development in modern microscopy include multiphoton fluorescence (two- and three-photon microscopy, generation of second harmonics), research with spatial resolution higher than the diffraction limit (nanoscopy), enhancement of the information content by additional measurements (fluorescence lifetime measurement and Raman spectroscopy), obtaining dimensional images at the organ and organismic levels, and the use of microscopy for clinical diagnostics.

2.1 Multiphoton microscopy

Endogenous fluorophores, such as collagen and elastin, are effectively excited in the wavelength range 400–450 nm, where the tissue absorption coefficient is high enough to limit the potential of single-photon microscopy for *in vivo* applications. Two-photon excitation partly eliminates this limitation because excitation light has a doubled wavelength ($\sim$ 800 nm) and the absorption in this spectral range is much lower. The quantum yield in multiphoton processes being proportional to the intensity of exciting radiation, the efficient generation of fluorescence requires a huge power density of the order of 1 MW cm^{-2} [11], attainable by using sharply focused femtosecond laser pulses [12]. An advantage of multiphoton over single-photon microscopy is the improved point spread function (PSF) with the structure practically devoid of sidelobes due to a rapid decrease in the fluorescence intensity far from the focus.

A commercial confocal laser scanning multiphoton microscope for *in vivo* research was created by JenLab GmbH (Germany). Such microscopes are used for *in vivo* studies of stem cell migration in the tissues of laboratory animals [13] and for clinical diagnostics of skin diseases [14, 15].

The application of multiphoton microscopy of biotissues is usually confined to the investigation of two-photon processes. However, the first reports on the use of three-photon microscopy of living objects published three years ago presented images of the neuronal network labeled with a red fluorescent protein at a depth of 1.2 mm in the brain of a laboratory animal; excitation at a wavelength of 1700 nm ensured a resolution of around 5 μm (Fig. 3). Such a large imaging depth with a microscopic resolution was possible due to the local water absorption minimum at this wavelength

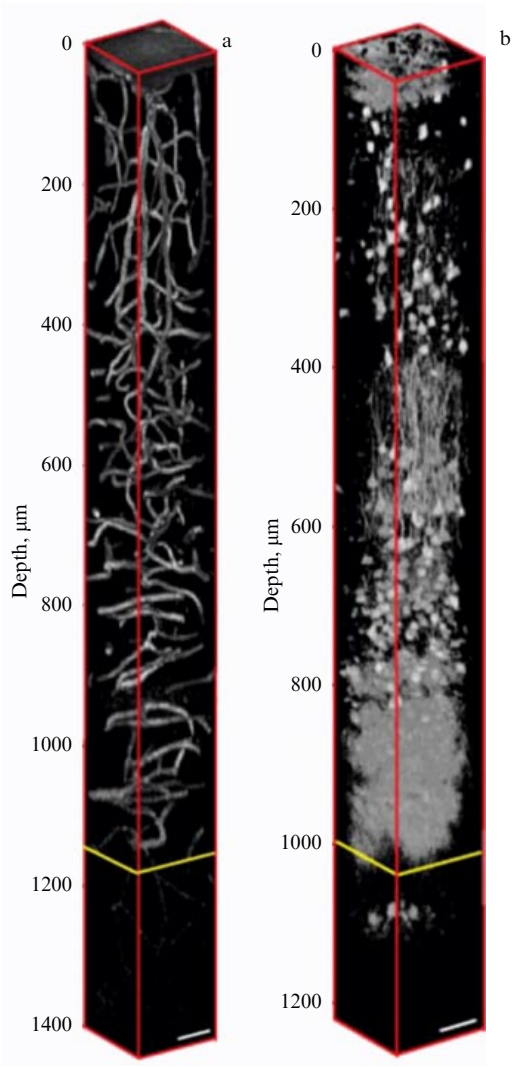

Figure 3. Three-photon microscopy of a mouse brain: (a) vascular system after administration of Texas Red dye, (b) the neuronal network expressing red fluorescent protein tdimer2 [16]. (Reproduced with permission of Macmillan Publishers Ltd., © *Nature Photonics*, 2013).

with the scattering coefficient roughly one third that in the case of excitation in the wavelength range 800–900 nm traditionally used in two-photon microscopy. Thus, although the exciting radiation with a wavelength of 1700 nm attenuates faster than the 800–900 nm radiation, its beam structure remains intact at much larger depths. Moreover, the emission spectrum of red fluorescent proteins lies in the red range, where the absorption coefficient is relatively small, which ensures the efficient reception of fluorescence.

2.2 Nanoscopy

Spatial resolution corresponding to the diffraction limit was reached in microscopy long ago. Interference methods (I^5M and 4Pi-microscopy) improved the spatial resolution by a factor of 5–7 (roughly 100 nm) in comparison with traditional confocal microscopy [17]. However, interference techniques did not find wide application due to difficulties of visualization caused by variations of the refractive index in biological objects.

A breakthrough in this field coincided with the advent of microscopy based on STimulated Emission Depletion (STED) [18]. In this method, a short pulse exciting fluorescence in the study object is followed by a STED pulse with a wavelength in the range corresponding to the fluorophore emission spectrum. The spatial distribution of the STED pulse is such that the intensity in the beam center falls to zero. Stimulated emission occurs in regions with a high intensity of STED pulses, i.e., in regions with depleted fluorescence. The higher the energy of a STED pulse is, the smaller the fluorescence region in the center of the beam where stimulated emission is absent and spatial resolution is increased. This method made it possible to reach a spatial resolution of 25 nm, or 25 times that of confocal techniques.

The traditional Abbe formula describing the resolving power of a microscope Δr corresponding to the diffraction limit at the wavelength λ and the objective numerical aperture NA,

$$\Delta r = \frac{\lambda}{2\mathrm{NA}}\,, \tag{1}$$

turns in STED microscopy into the relation

$$\Delta r_{\mathrm{STED}} = \frac{\lambda}{2\mathrm{NA}\sqrt{1 + I_{\mathrm{STED}}/I_{\mathrm{sat}}}}\,, \tag{2}$$

where $I_{\mathrm{STED}}/I_{\mathrm{sat}}$ is the ratio of the maximum STEAD-pulse intensity to the fluorophore saturation intensity.

Subdiffraction visualization is possible by virtue of an enormously high signal/noise (S/N) ratio obtained by application of short-pulse excitation and the detection of fluorescence with single-photon sensitivity. Depletion of fluorescence outside the excitation beam axis improves the spatial resolution but decreases the S/N ratio. Methods for improving the spatial resolution at a high S/N ratio are used, for example, in remote sensing with special signal processing algorithms; in STED microscopy, however, the diffraction limit is overcome at the instrumental level.

Another nanoscopic modality is STochastic Optical Reconstruction Microscopy (STORM), using photoactivated labels whose fluorescence can be 'switched on' (activated) by irradiation at a certain wavelength lying outside the excitation spectrum [19]. The intensity of an exciting laser is chosen such that only a few molecules are active simultaneously. Because the transition to the active state is a stochastic uncorrelated process, the probability of the presence of other active molecules within the radius of the diffraction spot around a fluorescent molecule is negligible. If the number of pixels per diffraction spot in the photodetector is sufficiently large, this a priori information permits finding the geometric center of the diffraction spot, which is regarded as the position of the fluorescent molecule. Finding such centers is a periodic process repeated every time after the molecules are first inactivated and then reactivated in a stochastic manner by the exciting laser. Such a process of collecting data about fluorescent molecule centers is a statistical procedure that takes much time to construct their distribution. The drift of fluorescent molecules in the course of data collection may distort the images. A group headed by G V Gelikonov at the Institute of Applied Physics, Russian Academy of Sciences, developed a new method to compensate such drift, using the data obtained without special fluorescent markers on the images (Fig. 4).

The creators of nanoscopy S Hell (Germany), E Betzig, and W Morner (USA) were awarded the 2014 Nobel Prize for

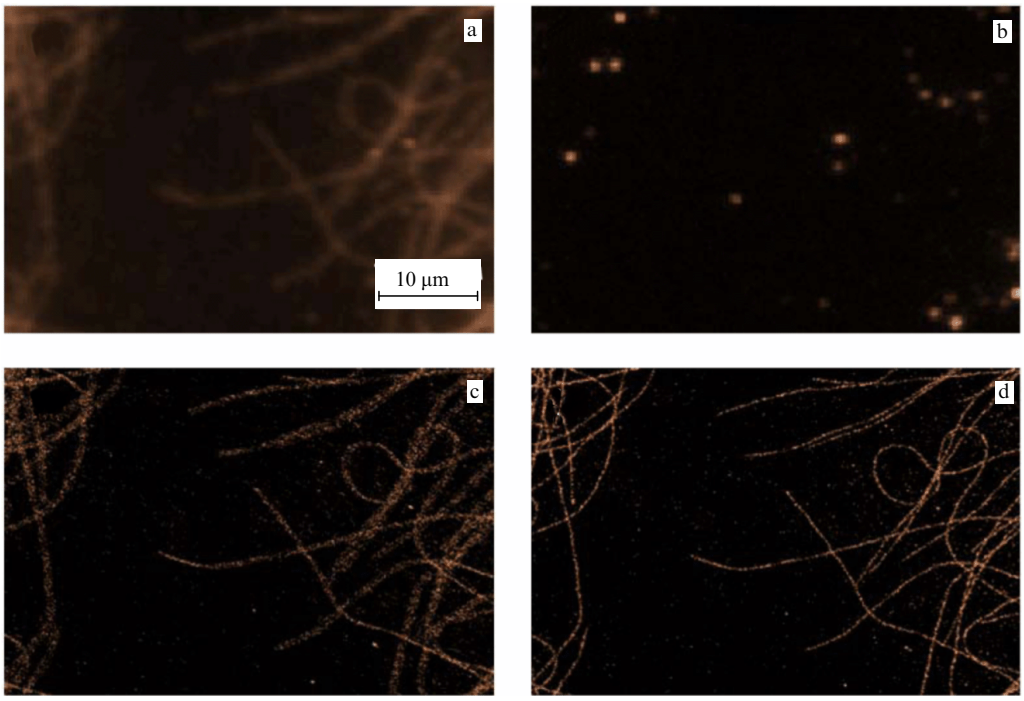

Figure 4. Application of drift compensation in STORM microscopy. (a) Image of Alexa 647-stained tubulin obtained by fluorescence wide-field microscopy. (b) The same object after administration of STORM buffer solution. Isolated fluorescent areas correspond to individual fluorophore molecules. (c) Image of the initial object obtained by the STORM method as described in Refs [19, 20]. Image smearing due to the particle drift during data acquisition. (d) Result of the drift compensation. The accuracy of molecule localization is roughly 25 nm at the initial resolution of wide-field microscopy of 220 nm.

"the development of super-resolved fluorescence microscopy."

One more way to overcome the diffraction limit for spatial resolution is based on structured illumination of a study object (by patterns having a definite structure) followed by image registration with the help of structured-illumination microscopy (SIM). The structure of the illumination field (patterns) is usually periodic with alternating dark and light interference lines. In the **k**-space (spatial frequency plane), the initial image obtained with the use of uniform irradiation occupies a circle with the radius k_0 corresponding to the diffraction limit. Each image obtained with a pattern occupies a region in the **k**-space shifted with respect to the origin by a vector $\mathbf{k}_1$ determining the pattern spatial frequency. The circle with the radius $k_0 + |\mathbf{k}_1|$ can be filled by patterns rotated with respect to each other. Integration of the images obtained with the use of different patterns results in an image with subdiffraction resolution in the **k**-space. At $|\mathbf{k}_1| = k_0$, the resolution in this space is two times higher than the diffraction limit. The authors of Ref. [21] argue that nonlinear excitation of fluorescence allows increasing the resolution by a factor of four or more.

Each of the above nanoscopic techniques for the investigation of biological structures has advantages and disadvantages, described in detail in Ref. [22].

2.3 Optical projection tomography and light-sheet fluorescence microscopy

Certain biomedical problems require elucidating the structural and functional organization of relatively small (invertebrates, fish) or large (biotissue samples, embryos) optically cleared biological objects on a scale comparable with their size. Optical methods for such visualization with cellular resolution were proposed not long ago. They are being further developed along two lines: optical projection tomography (OPT) [23] and light-sheet fluorescence microscopy (LSFM) [24]. The latter method is being rapidly developed in two versions: selective plane illumination microscopy [25] and ultramicroscopy [26]. The main difference between LSFM and traditional confocal laser scanning microscopy or wide-field microscopy is that fluorescence is excited only in a thin layer of a biotissue due to the use of special illumination systems and registration of fluorescence in the direction orthogonal to the plane of illumination. This allows direct laser radiation to enter the receiving channel and parasitic background illumination outside the region of interest to be avoided; in this way, three-dimensional images of large optically cleared biological objects can be obtained (Fig. 5).

3. Optical coherence tomography

Optical coherence tomography (OCT) is based on low-coherence reflectometry. The study medium is probed by a broadband radiation source, and the scattered light coming back from different depths with different time lags relative to the incident radiation is detected by an interferometer [28]. As in many cases of remote sensing, e.g., by radiolocation or ultrasound, the longitudinal resolution in OCT is inversely proportional to the radiation bandwidth, while the transverse resolution is determined by the directional diagram of the receiving and transmitting antenna. Femtocorrelated radiation sources, such as femtosecond lasers, superluminescent diodes, and supercontinuum laser sources, have been used to design OCT devices with a longitudinal resolution of 1–10 μm. This resolution is several times better than that of modern high-frequency apparatuses for ultrasound studies

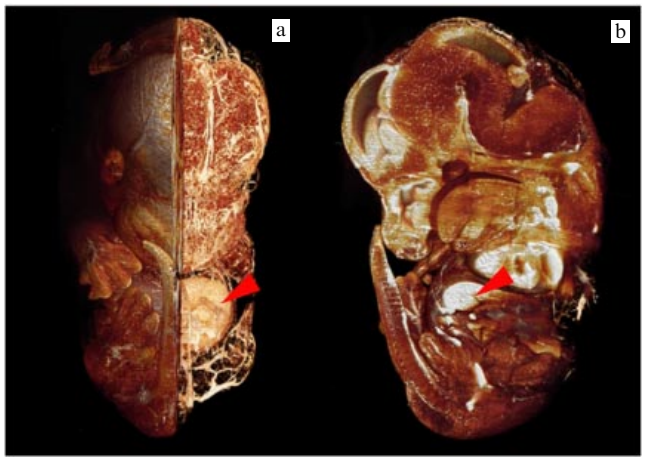

Figure 5. (Color online). 3D visualization of the structure of a 14-day-old mouse embryo in different projections (excitation at a wavelength of 488 nm, detection of autofluorescence). Red arrow shows the liver region [27].

(USSs). Because such a resolution corresponds to the cell size, OCT is not suitable for visualizing subcellular structures (except those in very large cells, e.g., plant cells) but allows tissue layers to be fairly well distinguished. This is of primary importance for obtaining intravital information about the internal structure of complex biotissues (e.g., eyeballs, skin, mucous and serous membranes of internal organs) needed to address a number of human health problems. Specifically, OCT of the retina is a standard diagnostic tool in ophthalmology, making it possible to detect early changes to vision [29–31].

Today, OCT is increasingly more widely applied in clinical practice for diagnostics of both malignant neoplasms [32] and benign pathology [33, 34]. In fact, OCT is becoming the method of choice for the management and treatment of patients with various diseases [35, 36].

The imaging depth in OCT is usually 1–2 mm, which corresponds to a roughly 40–50 dB change in the signal (equivalent to the device dynamic range). The most exact analytic expressions describing attenuation of an OCT signal (A-scan) with depth were derived in the small-angle approximation of the RTE [37, 38]. The relations thus obtained show that attenuation of the probing beam at a depth of 1–2 mm occurs much more slowly than in the Bouguer–Lambert–Beer (BLB) law

$$I \sim \exp\left[-(\mu_a + \mu_s)\, r\right], \tag{3}$$

according to which a singly scattered photon leaves the beam faster than in the diffuse approximation of the RTE:

$$I \sim \frac{\mu_s'}{r} \exp\left[-\sqrt{3\mu_a(\mu_a + \mu_s')}\, r\right], \tag{4}$$

where the isotropized beam attenuates as a result of absorption. In relations (3) and (4), μ_a and μ_s are the absorption and scattering coefficients, μ_s' is the transport (or reduced) scattering coefficient, and r is the distance from the source. The BLB law can also be realized in OCT (given an optically narrow beam [39]) but only at small depths. An OCT signal proper forms on photons backscattered by a biotissue. Inasmuch as the probability of backscattering is small, it can be regarded as a single event at a depth of 1–2 mm.

3.1 Clinical applications of optical coherence tomography

An indisputable advantage of OCT is the possibility of constructing all-fiber devices and miniature OCT probes for examining difficult-to-access organs and tissues. The aforementioned group headed by Gelikonov developed OCT probes with a diameter of 2 mm compatible with the biopsy channel of standard endoscopes for examining mucous membranes of respiratory, digestive, and urogenital organs [40]. Numerous clinical studies have demonstrated that the transformation of intact mucosa into a malignant neoplasm is associated with a change in its layered organization, i.e., distortion of the clear-cut boundary between epithelium and stroma (in agreement with results of histological studies). As a consequence, an OCT image of tumor is structureless (Fig. 6) [41, 42].

It follows from the foregoing that OCT permits accurately determining the border of a tumor, thereby avoiding a standard biopsy study taking much time and expense. It is especially important for planning the extent of surgical procedure and intraoperative control during organ-preserving surgery [43, 44]. True, OCT cannot totally substitute the 'golden standard' (biopsy) because it is not fit for detailed differential diagnostics. For example, it fails to reliably distinguish between inflammation and malignant neoplasm. Therefore, OCT needs to be further improved to provide additional clinical information [45].

The diagnostic value of the method was enhanced by its modification into polarization sensitive OCT (PSOCT) based on the use of polarization-maintaining fibers. It is known that various biological structures not only scatter optical radiation but also depolarize it and even rotate the polarization plane. Polarization effects are especially well apparent in collagen fibers and cartilage. Derangement of the collagen structure frequently associated with malignant growth leads to impairment of depolarization that can be visualized by PSOCT [46].

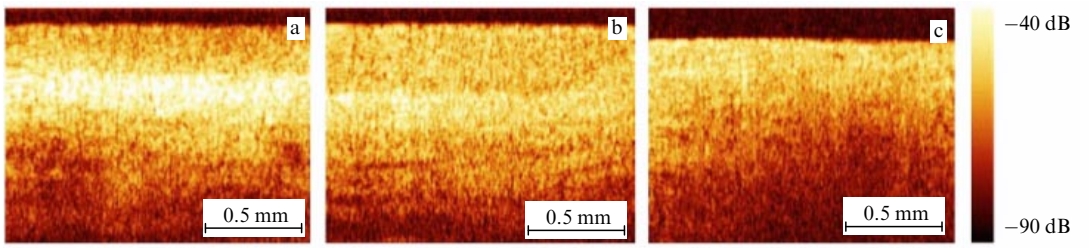

Figure 6. OCT images of uterine cervix: transition (a) from normal tissue (b, c) to the center of the malignant tumor.

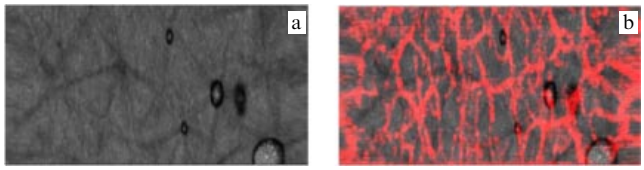

Figure 7. (Color online). (a) C-scan of breast skin obtained in vivo by OCT. (b) The same scan with the superimposed vascular pattern (red) obtained by analysis of speckle structure dynamics as described in [47]. The OCT image size 3.3 × 1.0 mm.

3.2 High-frequency optical coherence tomography and analysis of speckle structure

The transition from the traditional time-domain OCT to Fourier-domain OCT and spectral-domain OCT substantially accelerated the scanning process. These high-speed modes made it possible not only to obtain video information but also to observe the dynamics of the speckle structure. They are of special value for vascular structure visualization deep in the tissues, which is impossible by conventional OCT. The movement of blood cells in the vascular bed changes the speckle structure in the respective area of the OCT image. Due to this, the analysis of the speckle structure dynamics reveals a vascular structure (Fig. 7). The correct analysis is possible if the speed of OCT visualization is so high that the speckle structure in the tissues surrounding blood vessels has no time to develop appreciable changes under the effect of spontaneous motion of the tissues always taking place in biological objects.

To recall, speckle correlometry for microcirculation research has a rather long history [48], but only two-dimensional surface images have been available until recently. Three-dimensional information became obtainable only with the advent of high-speed OCT.

3.3 Spectroscopic optical coherence tomography

Because the longitudinal spatial resolution of OCT is proportional to the coherence length of probe radiation, it is necessary to use broadband sources, either pulsed (femtosecond lasers) or quasi-continuous (superluminescent diodes, arc lamps, incandescence bulbs). In most cases, however, it is impractical to use super-broadband sources having a bandwidth comparable to the central frequency. Even small dispersion of the medium refractive index uncompensated in the interferometer can be responsible for a big difference between phases gained by harmonics separated by a wide frequency range and coming from the same depth. The result is a smeared correlation function of the probing and detected signals.

The use of super-broadband sources, such as supercontinuum and frequency-tunable femtosecond lasers, allows spectroscopic OCT, providing additional data about a study subject. OCT images obtained with the use of relatively narrow (10 nm) bands in neighboring spectral ranges contain information on the spectrum of the extinction coefficient depending on scattering and absorption coefficients of the biotissue containing information about the study object [50]. To the best of our knowledge, this method has not yet found wide practical application.

3.4 Optical coherence microscopy

While the longitudinal resolution of OCT is a function of the radiation source bandwidth, its transverse resolution depends on the probing beam geometry. The high numerical aperture of the output lens, as in confocal microscopy, allows creating a diffraction spot of minimal size. However, such fine focusing is associated with a small depth of Rayleigh length, which prevents observation of the biotissue structure with a high transverse resolution outside the focal zone. In other words, there is an optimal focusing for each imaging depth. A high transverse resolution at all depths down to 1–2 mm is attainable by dynamic focusing, i.e., by combining OCT with confocal microscopy or so-called optical coherence microscopy (OCM).

Visualization of biotissues by OCM has been reported by several research groups [51–53], but this method is not yet used in endoscopy, because dynamic focusing requires large scanners with a lens-positioning mechanism and increases the scanning time.

3.5 Contrast enhancement in optical coherence tomography

It is worthwhile to mention avenues of OCT development aimed at improving the contrast and imaging depth. The group headed by V V Tuchin at Chernyshevskii Saratov State University investigated the optical clearing effect and showed that the use of agents such as glycerol, propylene glycol, and strong glucose solution allows increasing the OCT probing depth and image contrast due to the ability of hyperosmolal substances to selectively correlate the refractive indices of background structures and scattering objects and thereby decrease the scattering potential of tissue components [54, 55].

Another area is the application of contrast agents, such as gold and titanium dioxide nanoparticles, that have a large scattering cross section. Their selective distribution after surface application enhances the contrast of biotissue structural elements [56, 57].

3.6 Automatic detection of diseases by analyzing optical coherence tomography images

The huge amount of clinical material collected with the help of OCT and confirmed histologically provides a basis for the development of automated methods for the assessment of pathological conditions of biotissues of a given localization. Some of these methods are designed to evaluate scattering and backscattering characteristics of layered tissue structures [39, 58] using various analytic approximations of the RTE, while others are based on the calculation of the parameters of the OCT-image texture. The automatic analysis of the OCT-image texture made it possible to increase the diagnostic accuracy of the method used to detect Fallopian tube pathology from 88 to 96% [59].

4. Optoacoustics

The spatial resolution of purely optical imaging techniques is confined to scattering effects at depths larger than 1 mm. This limitation motivated researchers to develop hybrid optical methods combining optical and other principles of visualization. The greatest progress was achieved in optoacoustics (OA). OA visualization is based on the detection of ultrasound pulses excited in a study medium upon absorption of pulsed laser radiation by biotissue chromophores [60]. The exited OA pulses have a small amplitude up to 10 kPa and a broad band of a few tens of MHz. OA pulses are recorded on the medium surface using ultrasound antennas with mechanical or electronic scanning as in standard USS.

4.1 Imaging depth in optoacoustics

The imaging depth in OA research is determined by the parameters of optical and acoustic attenuation in biotissues, the energy of laser pulses, the sensitivity of the receiving system, and the absorption coefficients of exogenous and endogenous chromophores. Moreover, the imaging depth of OA greatly depends on the wavelength, because the optical absorption coefficient of a biotissue also depends on the wavelength. Evidently, the imaging depth in the therapeutic transparency window is much greater, for example, than in the blue or green spectral ranges. At the same time, the absorption coefficient of a chromophore being visualized should be taken into consideration, because the OA signal is proportional to this parameter. For example, the absorption coefficient of hemoglobin (a major tissue chromophore) is much higher in the green spectral range than in the therapeutic transparency window. Therefore, the amplitude of OA-signal generation during visualization of vascular patterns in surface tissue layers (3–4 mm) is higher in this wavelength range.

To reach the largest depth of OA visualization of a few centimeters, the 700–900 nm wavelength range should be used, in which biotissue absorption is minimal, along with the maximum allowable energy of the laser pulse; also, maximum sensitivity of the detector must be ensured. For example, an imaging depth of more than 4 cm was reached during *in vivo* breast examination with a 800 nm laser [61]. Because the absorption coefficient of hemoglobin in this spectral range is relatively small, the OA signal (and therefore the imaging depth) can be increased by using contrast agents with high absorption coefficients in this range, such as methylene blue, indocyanine green, or gold nanoparticles with plasmon resonance [62, 63].

4.2 Spatial resolution in optoacoustics

Similarly to USS, the depth resolution of OA is a function of the spectral bandwidth of the acoustic signal being detected, while the transverse resolution depends on the aperture of the acoustic antenna and its focusing properties. Because the acoustic absorption coefficient of biotissues is inversely proportional to the wavelength, the number of elements of ultrasound (US) resolution in an A-scan is the same for short-wavelength (high-frequency) and long-wavelength (low-frequency) acoustic antennas. Additional factors worsening spatial resolution are the finite length of the probe pulse and the limited working bandwidth of the receiving antenna. A 20 ns probing pulse restricts generation of an US pulse at the frequencies above 50 MHz US, which exceeds the potential of OA visualization for depths greater than 1 mm. Higher-frequency receivers and shorter light pulses are needed for investigations at smaller depths. Although the spectral band of classical acoustic antennas does not exceed the central band, some acoustic sensors based on optical interferometers have a much broader spectral band [64]. The sensitivity of the existing optical resonators is still below that of traditional acoustic antennas.

4.3 Chromophore separation in optoacoustics

An advantage of OA visualization over USS is not only the enhanced contrast but also the possibility of spectroscopic measurements for the identification of individual tissue chromophores. OA visualization is performed with the use of lasers tunable in a broad wavelength range. Similarly to diffuse optical spectroscopy, OA spectroscopy allows estimating the degree of blood oxygenation, identifying exogenous contrast agents with resonant absorption, etc.

Estimation of the concentration of various chromophores from spectroscopic data requires measuring the biotissue absorption coefficient and correctly taking the optical fluence distribution inside the tissue into account because the amplitude of an OA signal is proportional to the optical fluence of a given area of the medium, differing for different wavelengths. This problem has been encountered by many researchers, but there are thus far no stable algorithms, e.g., for assessing the blood oxygenation. To assess the optical fluence distribution, it is proposed to combine OA spectroscopy and diffuse optical tomography (DOT), allowing the evaluation of scattering and absorption coefficients for determining the optical field inside the medium. But this approximation requires additional measurements, which complicates the construction of the device and (more importantly) increases the geometric size of its scanning system. An original resolution of this difficulty was proposed in Ref. [65], where backscattered light was detected by an acoustic antenna designed to receive US pulses. To use this information for calculating the optical fluence distribution, the complicated problem of three-dimensional DOT reconstruction must be resolved.

4.4 Optoacoustic microscopy and tomography

There are a variety of technological solutions for OA visualization of biotissues, which can be arbitrarily categorized into tomographic and microscopic. OA tomography implies recording US pulses by a multielement antenna or several spaced antennas simultaneously with the reconstruction of the absorbing inhomogeneities in biotissue [66, 67].

In OA microscopy, A-scans are registered by a single US sensor used for one- or two-dimensional scanning along the object surface.

The main advantage of tomography is the absence of mechanical scanning by a sensor, which increases the OA visualization speed in comparison with microscopy; this OA feature is of primary importance for clinical studies. However, a tomographic system is very expensive due to the use of a complex multielement antenna, multichannel analog-to-digital converter (ADC), and reconstruction algorithms. AO tomography is possible with the use of an array of acoustic antennas (by analogy with standard US diagnostics) or a two-dimensional multielement antenna [63, 68]. These are the most universal systems that can be used to examine practically any open part of the body without limitations on the thickness of the study object. It is possible to design a tomographic system for a given object geometry with several US sensors fixed on the object surface. Such systems were created for diagnostics of breast pathology [69, 70] and tomography of small laboratory animals [71].

OA microscopy is a relatively inexpensive version of OA visualization designed for the following studies: optimization of systems for laser illumination of biotissues with a view to creating a uniformly deep optical field or achieving a higher spatial resolution [72]; the search for various materials and amplifiers for acoustic antennas; and evaluation of new opportunities for OA visualization and simultaneous generation of OA and US images [73–75] (Fig. 8). The high cost of tomographic systems (around 700,000 EU) hampers the conduct of extensive clinical trials and application of this imaging technique in routine clinical practice. Therefore, less

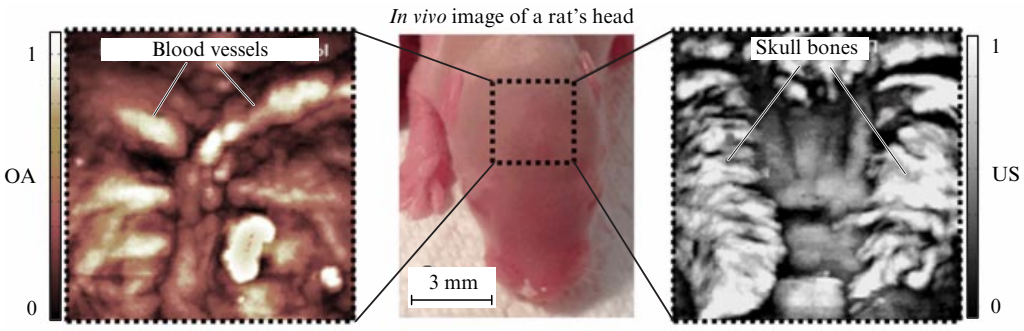

Figure 8. (Color online). *In vivo* optoacoustic (OA) and ultrasound (US) images of a 3×3 mm part on the head of a 3 day-old rat. Scanning pitch is 30 μm, imaging time is 20 min [78].

expensive high-speed systems for OA microscopy [76] may be more in demand at the present stage of development of this method. Moreover, there is a class of intravascular OA-visualization systems in which a rotating US sensor is used (as in US diagnostics of vascular problems) because of the impossibility of accommodating a large multielement antenna.

4.5 Biomedical applications of optoacoustics

OA visualization has a huge potential for investigations of animal models. There are commercial systems for the so-called real-time 5D monitoring of various processes, e.g., elucidation of spectrally and temporally resolved volumetric distribution of chromophores. Such systems are indispensable for studies in experimental oncology, developmental biology, pharmacokinetics and pharmacodynamics, etc. Small laboratory animals are most suitable for the purpose of OA visualization because the thickness of their body corresponds to the maximum imaging depth. Therefore, this method can be used for whole-body imaging, similar to traditional CT and MRI.

However, progress in clinical OA applications is much slower, probably due to the lack of clinical data confirming the diagnostic efficiency of the method in various fields of medicine.

The most promising clinical applications of OA imaging are as follows [79]:

— diagnostics of breast cancer from enhanced vascularization revealed by OA visualization of tumor vasculature [80];

— monitoring of tumor growth and treatment response by OA measurements of blood oxygenation in the surrounding vessels [81];

— targeted biopsy of signal lymph nodes with the use of exogenous light-absorbing markers [82];

— diagnostics of melanin-containing neoplasms to facilitate preoperative preparation and surgical removal of the tumor by simultaneous OA visualization of skin blood vessels and melanoma [83];

— studies of brain hemodynamic reactions to external stimulation and observation of epileptic symptoms by OA visualization of cerebral vessels with simultaneous evaluation of blood oxygenation [84];

— diagnostics of atherosclerotic changes in main blood vessels by OA visualization of cholesterol and calcium deposits [85];

— diagnostics of age- and diabetes-related impairment of vision by OA imaging of retinal vessels with the evaluation of their oxygenation status [86].

5. Diffuse optical spectroscopy and tomography

5.1 General information on diffuse optical spectroscopy

Diffuse optical techniques are based on registering the multiply scattered diffuse component of light after it passes through a layer of biotissue and solving the inverse problem of reconstructing its scattering and absorption coefficients [87]. The table shows that diffuse optical methods ensure a deeper visualization of biotissues (down to 10 cm) than other optical techniques for the same purpose, because diffuse light propagation in the tissue has the smallest attenuation factor (4), which contains the product of transport scattering and absorption coefficients (in the therapeutic transparency window $\mu_a \ll \mu_s'$). This means that the optical fluence that passes through a biotissue is equally sensitive to a change in each optical characteristic. The scattering coefficient changes only insignificantly, depending on the wavelength, typically in accordance with the power law λ^{-b} where b is 0.5–1.5 [88].

The spectrum of absorption coefficients depends on concentrations of various chromophores present in biotissues (oxy- and desoxyhemoglobins, water, lipids, collagen) (see Fig. 1). Measurement of the spectrum of absorption coefficients gives concentrations of these chromophores with well-known partial spectra. As a rule, concentrations of oxy- and desoxyhemoglobins are measured; their ratio characterizes the blood oxygenation status. More accurate spectroscopic measurements allow determining water, hemoglobin, and collagen content. Spectroscopic measurements in the wavelength range 935–998 nm give the bound water content [89]. All these parameters, including the scattering coefficient, are of diagnostic value and can be used as indicators of malignant growth. Specifically, concentrations of water n_{H_2O} and blood n_{THb} (total hemoglobin mass) increase, while the degree of oxygenation StO_2 decreases in the presence of a tumor.

It was shown that knowledge of a single diagnostic parameter is not enough to make a definitive conclusion about the presence or absence of a tumor because its values in normal and pathologically changed tissues may overlap. The so-called tissue optical index (TOI) taking all measured parameters into account was proposed in [90]:

$$\mathrm{TOI} = \frac{n_{\mathrm{THb}}\, n_{\mathrm{H_2O}}}{n_{\mathrm{lipid}}\, \mathrm{StO_2}}, \qquad (5)$$

which reflects a much greater contrast enhancement in the presence of pathological changes.

5.2 Continuous wave, time-domain, and frequency-domain approaches in optical diffuse spectroscopy

As was mentioned in Section 5.1, knowledge of the scattering coefficient spectrum is needed to correctly reconstruct the component composition of a biotissue. In most cases, tabulated values of this parameter for different types of biotissues are not enough to reconstruct the component composition, even though scattering variations are not so conspicuous as those of absorption. Therefore, additional measurements are needed to determine the scattering coefficient.

The most consistent separate estimation of scattering and absorption coefficients is obtained by frequency-domain or time-domain methods [91]. Because DOS registers the multiply scattered light component, its time delay with respect to the probing pulse is much longer than that of the ballistic component propagating directly from the source to the detector. This delay can be determined either by measuring the phase shift in the frequency-domain approach or from the overall time distribution of photons in the time-domain method. Using these measurements and the measured extinction coefficient in a biotissue, it is possible to estimate the scattering and absorption coefficients separately [92].

Both methods have advantages and disadvantages [93]. The frequency-domain approach is realized by means of high-frequency modulation (of the order of 100–500 MHz) of the probing radiation intensity followed by synchronous reception of diffuse photons. This method is relatively inexpensive, but sophisticated high-frequency electronic equipment and a large modulation depth of the laser source are needed for stable signal detection and the phase separation measurements with an accuracy reaching tenths and even hundredths of a degree. The time-domain method is much easier to implement, but its instruments (pulsed pico- or nanosecond lasers and time-correlated single-photon counters) are very expensive. The time-domain approach traditionally provides much more information about a study object: a detected pulse expanded in the Fourier series is a set of amplitudes and phases that can be obtained by the frequency-domain method at different modulation frequencies.

Separate determination of scattering and absorption coefficients is also possible with the use of a continuous radiation source, but measurements must be made at several points located at different distances from the source. The accuracy of separate determinations of these parameters in such systems is much lower than by the frequency-domain and time-domain methods. An important advantage of continuous broadband radiation generated by halogen or arc lamps is the possibility of simultaneous registration of the optical spectrum with the help of an ordinary spectrometer.

The research group headed by Tromberg developed an original system combining the advantages of frequency-domain and continuous wave spectral approaches [94]. Bearing in mind that the scattering coefficient is fairly well approximated in the whole spectrum by a power-law wavelength dependence, it can be determined by the frequency-domain method with measurements at several points of the spectrum, i.e., by using a small number of laser sources with intensity modulation. Characteristics of the scattering coefficient obtained with the help of modulated sources and of the light attention coefficient over the entire spectral range obtained with a continuous broadband source can be used to reconstruct the concentration of all the main chromophores of the biotissue.

5.3 General information on diffuse optical tomography

DOS is applied under the assumption of the uniformity of optical characteristics in the study medium, which restricts the accuracy of the reconstruction of tissue chromophore concentrations and does not allow evaluating their spatial distribution. Diffuse optical tomography (DOT), unlike DOS, allows reconstructing the spatial distribution of scattering and absorption coefficients [95]. DOT is based on obtaining projections, i.e., information on optical radiation that passes through a biotissue at different positions of the source and the detector, with subsequent application of reconstruction algorithms [96–98].

Reconstruction algorithms are based on the assumption that a biotissue is characterized by certain mean values of optical parameters, such that deviations from these values in different regions of a study medium are relatively small. It permits expanding the RTE solution in the diffuse approximation in a Taylor series and is confined to linear corrections with respect to scattering and absorption coefficients. This transition reduces the problem of finding the spatial distribution of optical parameters to a system of linear equations with the sensitivity matrix of size $M \times N$, where M is the number of lines (projections) and N is the number of voxels in which corrections for optical characteristics are evaluated.

Reconstruction algorithms in DOT are continuously improving and have many modifications for the solution of both direct and inverse problems. A complication arises from the necessity of taking the medium geometry into account, from the ill-posedness of the DOT problem, and sometimes from a limited applicability of the diffuse approximation of the RTE. We discuss these problems and approaches to their solution in more detail in Sections 5.4 and 5.5.

5.4. Boundary conditions in diffuse optical tomography

The RTE solution is very sensitive to boundary conditions, because the optical fluence near the scattering medium–air interface increases due to reflection of photons from the boundary. For an infinite homogeneously scattering and absorbing medium, the diffuse approximation of RTE has a simple analytic solution. For a semi-infinite medium or a planar layer, this solution is readily modified by adding negative or image sources of photons to the infinite-medium problem in order to satisfy the boundary conditions. RTE solutions for a semi-infinite medium are used in both DOS and DOT for examining a small area of biotissue in the reflection configuration when the source and detector are placed on the same side of the study object (small scanners for breast examination and the study of activity in a small brain area).

In the case of a conventional boundary, more intricate numerical methods have to be used for the RTE solution; this complicates the algorithms considerably and increases the time for calculating the sensitivity matrix. Moreover, DOT with an 'antireflection' geometry, where the source and detector are placed on different sides of the object, is sometimes performed with the use of matching liquids (usually a lipofundin–Indian-ink mixture) having scattering and absorption coefficients similar to those of the biotissue. The matching liquid is poured into a rectangular cuvette and the study object is submerged into this medium. This method simplifies solving the problem but has a number of inconveniences when used in working with living objects. Therefore, its application is limited to diagnostics of breast pathology [99] and experiments on laboratory animals [100]. Reconstruction algorithms for arbitrary surfaces should be used in brain DOT.

5.5 Solution of the inverse problem of diffuse optical tomography

Researchers choosing to use DOT encounter a number of difficulties (absent in other transmission problems, e.g., X-ray tomography) when inverting the sensitivity matrix [101]. This matrix in DOT is nonsparse, poorly conditioned, and sometimes underdetermined. Nonsparseness is attributable to the diffuse character of light propagation: even when an absorbing or scattering inhomogeneity is outside the projection axis connecting the source and the detector, it still exerts influence on the signal being detected. Poor conditioning is likewise a consequence of diffuse light propagation: minor changes in the detected signal may result in a marked alteration of the reconstructed spatial distribution of optical inhomogeneities.

The above conditions dictate the necessity of measurements with a high degree of linearity and good signal-to-noise ratio, as well as obtaining comprehensive information about the study object, including its geometry. Also needed are more accurate models of light propagation near the boundary (where the diffusion approximation is inapplicable but the sensitivity to optical inhomogeneities is very high), the use of frequency-domain and time-domain approaches, and a large number of projections measured with a high degree of accuracy [102, 103]. Nevertheless, the instability of the solution of the inverse problem remains very high in the absence of additional information. Therefore, DOT should be combined with other methods, e.g., magnetic resonance imaging (MRI) or X-ray computed tomography (CT), which allows elucidating the biotissue structure with good spatial resolution. Determination of the object structure and surface geometry by these methods is followed by its segmentation, with optical characteristics in each segment being assumed constant. This allows a significant reduction in the number of unknowns in the inverse problem, thereby increasing the reconstruction accuracy and stability. Such an approach is used to study brain functional activity [104] and diagnose breast pathologies (Fig. 9) [105]. This means that purely optical methods generally fail to provide structural information at large depths (from a few millimeters) but allow extracting data on the functional state of a biotissue from the information obtained by other techniques.

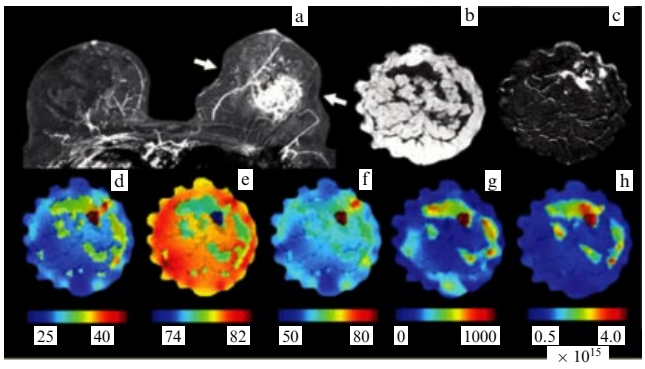

Figure 9. (Color online.) MRI and DOT breast studies. (a) T1-weighted breast images in the axial plane obtained by MRI with dynamic contrast enhancement (arrows show the plane in which DOT images were obtained). (b) T1-weighted breast images in the coronal plane in the projection of the tumor node prior to contrast administration. (c) Image constructed by subtraction from the data obtained after and before contrast administration. Reconstructed DOT images obtained with the use of MRI segmentation: (d) hemoglobin level (μmol l^{-1}), (e) oxygen saturation (%), (f) concentration of water (%), (g) size of scattering particles (nm), (h) concentration of scattering particles [105]. (Reproduced with the permission of OSA publishing.)

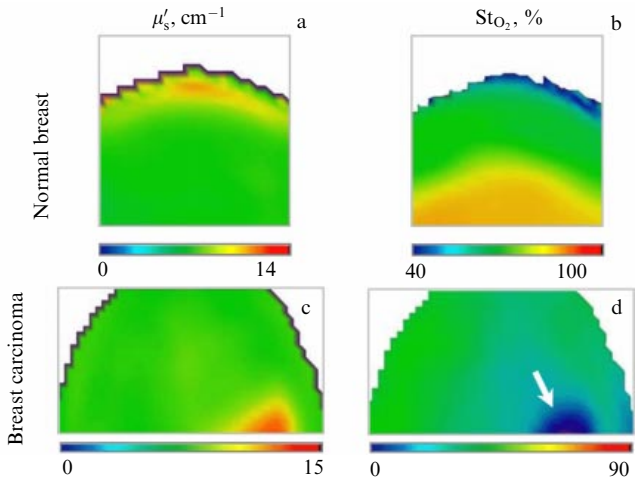

Figure 10. (Color online.) Optical mammography: determination of scattering coefficients and blood saturation with oxygen in a breast by DOS in antireflective configuration. (a, b) Normal breast (image size 50 × 50 mm). (c, d) Breast carcinoma shown by the arrow (image size 90 × 50 mm).

5.6 Other diffuse optical methods for the study of biological tissues

The necessity of optical images, on the one hand, and the difficulty of solving tomographic problems, on the other hand, motivate the development of DOS modifications that allow obtaining two-dimensional images of the absorbing and scattering inhomogeneities present in biotissues. For example, there are projection DOS systems with a trans-illumination configuration, besides manual scanners for diagnostics of breast pathology [106]. In such systems, with the source and the detector placed on different sides of the study object, the time-domain [107] or frequency-domain [108] approach is used. Similarly to X-ray mammography, this method, known as optical mammography, yields information about biotissue properties integrated over depth at each spatial position of the source and the detector (Fig. 10).

Another approach is based on structured illumination of biotissues and substitution of spatial frequencies for time modulation [109]. It is used to examine the surface layers of a biotissue (to a depth less than 1 cm) and, unlike the methods described above, does not require mechanical scanning of the object surface; due to this, imaging time is significantly reduced.

6. Macroscopic fluorescence imaging techniques

Fluorescence imaging techniques, both microscopic and macroscopic, provide data on the two- and three-dimensional fluorophore distribution in biotissues. A comparison of micro- and macroscopic methods in terms of imaging depth (1–2 photon mean free paths) shows that in the latter case, fluorophore excitation and/or detection of its fluorescence is performed by the scattering light component.

As mentioned above, both endogenous and exogenous fluorophores can serve as contrast agents. The endogenous ones are markedly excited only in the UV–blue region of the spectrum, where the light absorption coefficient is rather high

and the imaging depth is confined to that of multiphoton microscopy. For this reason, macroscopic fluorescence techniques largely operate with exogenous markers (organic dyes, fluorescent protein, synthesized nano-scale agents, etc.) excited in the red and near-infrared spectral range or having a very high brightness in the blue–green range. These methods are subdivided into surface, projection, and tomographic [110].

6.1 Surface fluorescence imaging techniques for the study of biological tissues

The most widely used surface methods are based on the excitation of fluorescence in a biotissue area of interest by a wide light beam and its detection by a digital camera with an optical filter that is transparent to fluorescence and blocks the excitation light. A modification of this technique is raster scanning based on the same principle as laser scanning microscopy, i.e., point-by-point scanning with a narrow light beam and simultaneous detection of fluorescence from a given area.

Raster scanning permits decreasing the influence of the scattering component coming from neighboring regions at each measuring point [111]. Due to a high fluorescence contrast, the surface methods yield a high-quality picture of the fluorophore distribution in the tissue. They are widely used in experimental oncology to observe the growth of a tumor labeled with fluorescent proteins (FPs), to study pharmacokinetics and pharmacodynamics of new fluorescent agents, etc. [112].

Clinical applications include intraoperative control during tumor removal [113, 114] and monitoring photodynamic therapy (PDT) with visualization using the fluorescence of a photosensitizer (PS) administered to patients [115, 116]. Low-intensity irradiation of PS does not cause a photodynamic reaction but PS fluorescence can be recorded in the tumor and the surrounding tissues. PDT is associated with photobleaching, i.e., a reduction in the PS fluorescence intensity, whose value can serve as a predictor of PDT efficiency [117].

6.2 Fluorescence tomography

Methods of fluorescence tomography use many projections of a study object irradiated from a fluorescence-exciting source and registration of emission with the subsequent reconstruction of the fluorophore distribution in the tissue. Fluorescence diffuse tomography (FDT) detects multiply scattered photons, and therefore faces the same problems as DOT, i.e., high sensitivity to boundary conditions, ill-posedness of the inverse problem, and limitations on the use of the diffusion approximation of the RTE.

However, the problem of reconstructing the fluorophore concentration, unlike that of reconstructing the absorbing and scattering coefficients, is solved more efficiently even in the absence of additional data on the object structure.

First, it has been shown that the conditioning number of the inverse FDT matrix is greater than in DOT because the fluorophore concentration being reconstructed is nonnegative [118].

Second, FDT provides the possibility of detecting not only fluorescence but also exciting radiation; the use of an additional source allows obtaining data on the passage of radiation through a biotissue in the fluorophore emission spectrum. These data permit normalizing the fluorescence signal and thereby reducing the influence of boundary conditions and variations of absorbing and scattering coefficients on the resultant solution (the so-called normalized Born approximation) [119]. Moreover, detection of fluorescence by a spectrometer enhances the accuracy of the reconstruction by the spectral FDT that uses the tissue absorption coefficient dispersion [120] (Fig. 11).

Third, FDT typically allows the reconstruction of the spatial distribution (presence or absence) of fluorophore rather than its concentration for determining the geometrical size and localization of a tumor labeled with a genetically encoded marker. This problem is easier to address once *a priori* information is available suggesting that the object (tumor) being reconstructed is simply connected. FDT is successfully used in experiments on laboratory animals using various fluorescent agents [121] and in diagnostics of breast pathology [122, 123] with the use of indocyanine green (ICG).

The FDT signal must be strong enough for the correct reconstruction of the fluorophore concentration, which is possible only with the use of markers whose excitation and emission spectra lie in the therapeutic transparency window. This condition restricts the use of FDT for green, yellow, and red fluorescent proteins. Far-red proteins, such as *Katushka*, *mCherry*, *mRasbery* etc., although fluorescent in the therapeutic transparency window, are excited in the yellow spectral region, where the tissue absorption coefficient is still sufficiently high [124]. The higher the absorption coefficient is, the more intense the background autofluorescence (i.e., tissue intrinsic fluorescence) that adds to the signal being detected and thereby deteriorates the reconstruction quality [125]. This addition can be subtracted by means of multispectral measurements at three to six different excitation wavelengths of an exogenous marker with well-known spectral characteristics [126]. Such a procedure may take much time (from 20 min to 1 hour), which is not always

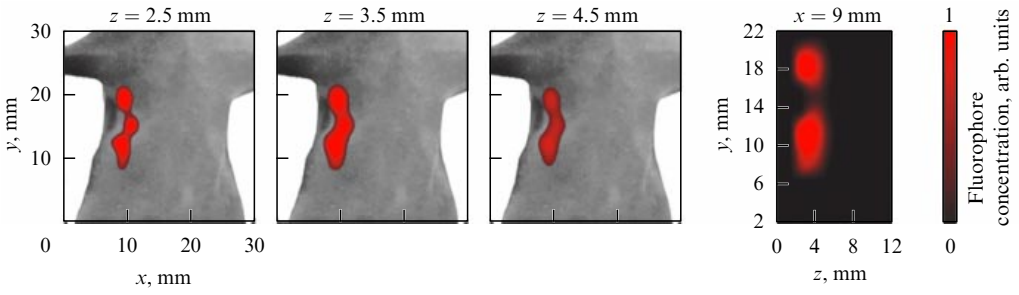

Figure 11. (Color online.) 3D reconstruction of the geometric size of the tumor expressing fluorescent protein Katushka in a nude mouse by spectral FDT: x, y — transverse coordinates, z — depth. The mouse's body surface is shown in grey color, the reconstructed fluorophore concentration in red.

allowable in *in vivo* experiments. To improve the FDT reconstruction quality, as with DOT, hybrid FDT–CT systems are created, combining fluorescence and X-ray tomography [127]. Studies of the distributions of biocompatible nanoparticles containing radionuclide and a far-red fluorochrome in laboratory animals by PET–CT and FDT–CT show good correlation between the results obtained by the two methods [128].

6.3 Fluorescence projection methods for the study of biological tissues

Because surface methods do not allow studying fluorescence deep inside biological tissues (down from a few millimeters) and tomographic techniques are too complicated and time-consuming, it is sometimes desirable to use an intermediate approach, e.g., the projection method realized by point-to-point scanning of a study object with the help of the source and the detector in a trans-illumination configuration (an analog of projection DOS). This method reveals the two-dimensional fluorophore distribution while the Born normalization practically excludes the influence of boundaries and inhomogeneities of the object optical characteristics.

The projection method yields especially good results when used to study deep-seated tumors labeled with far-red proteins [129].

6.4 Spectral and time-resolved separation of fluorophores

Separation of autofluorescence and fluorescence of one or several exogenous markers mentioned in Section 6.2 can be realized either by spectral or temporal methods based on the difference in the respective spectral (excitation and emission spectra) and temporal (relaxation time) characteristics of fluorophores.

Spectroscopic measurements are performed by rearranging the excitation wavelength of the source and/or emission filters of the detector. Excitation and fluorescence spectra being usually broad enough (a few tens of nanometers), it is very difficult to resolve fluorophores with similar spectral characteristics by this method. Measurement of the lifetime permits distinguishing between fluorophores with overlapping spectra and can be used to study intracellular processes *in vivo* by Forster resonance energy transfer (FRET) between fluorescent molecules [130, 131].

Temporal measurements became possible with the advent of short-pulse (nanosecond) laser sources and detectors based on a time-correlated single-photon counter or camera with an image intensifier based on a microchannel photocathode [132–134], allowing photon arrival time to be respectively resolved up to 1 or 200 ps.

Another way to determine fluorophore lifetime is from the phase shift between high-frequency (~ 50 MHz) intensity-modulated excitation light and the fluorescent signal being detected by analogy with the frequency-domain in DOS.

6.5 Fluorescent markers

Studies are currently underway designed to create new bright fluorescent markers excited in the near-infrared range. Of special interest among genetically encoded markers (fluorescent proteins) are the aforementioned far-red FP and near-infrared fluorescent proteins (iRFP) [135] with low brightness but with the excitation spectrum lying in the red range. Quantum dots are thus far not regarded as potential markers for *in vivo* studies, despite their high brightness and the possibility of generating narrow emission beams in the near-infrared range, because their potential toxicity remains virtually unexplored [136]. Indeed, indocyanin green is so far the sole fluorophore approved by the US Food and Drug Administration (FDA) for clinical applications in very low concentrations (the maximum allowable dose is 2 mg/kg, according to the instructions for use).

Worthy of note are extensively developed markers with anti-Stokes fluorescence [137], the so-called up-converting nanoparticles (UCNPs) having a higher-frequency emission spectra than the excitation spectrum. The spectral properties of these particles allow completely excluding autofluorescence of biotissues known to limit the sensitivity of fluorescent methods when fluorophores with the Stokes shift are used. UCNPs are characterized by nonlinear excitation; the quantum yield is proportional to the power density when it is relatively low (below $1\,\mathrm{W\,cm^{-2}}$), as in classical two-photon fluorescence, but its value can amount to several percent, which suggests the possibility of using nanoparticles for deep visualization [138–140]. The quantum yield is less dependent on the high power density, i.e., the saturation effect takes place.

Thus, anti-Stokes fluorescence permits excluding the influence of autofluorescence on the signal being detected, which restricts the imaging depth when using fluorescent agents with the usual Stokes shift. Moreover, nonlinear excitation of UCNPs can be used in FDT reconstruction algorithms for more accurate localization of these particles [141]. It was shown in Ref. [142] that UCNPs can be attached to scFv4D5 mini-antibodies for specific binding with HER2/neu receptors expressed in human SK-BR-3 adenocarcinoma cells; the imaging depth of these complexes in the breast can reach 4 mm.

6.6 Near-infrared fluorescence imaging

In the past three years, fluorescence macroscopy, similarly to microscopy, has extensively employed new spectral wavelength ranges between 1200 and 1700 nm, where the water absorption coefficient has a local minimum and scattering coefficients are several times lower than in the 700–900 nm range traditionally used for deep fluorescence visualization.

For example, *in vivo* surface fluorescence imaging with the use of single-wall carbon nanotubes administered intravenously revealed the structure of the cerebral circulation system in laboratory animals at a depth up to 3 mm with a 10 μm resolution in the NIR-2a (1300–1400 nm) range [143].

7. Conclusion

It follows from the foregoing that optical methods are being extensively developed to visualize biological objects at various levels, from nanoscopy resolving individual molecules to whole-body imaging of laboratory animals and human organs. The images are constructed depending on the method in use, based on varying parameters, such as biotissue absorption and scattering coefficients and the brightness of endogenous and exogenous fluorophores.

The use of fluorescent and absorbing markers makes optical methods attractive for the study of molecular processes. However, they cannot compete with traditional PET and MRI of large objects due to the limited imaging depth. This accounts for the great attention given to the synthesis of new bright fluorescent agents having emission and absorption spectra in the biotissue transparency window. Specifically, the fluorescent protein iRFP has been obtained

to serve as a genetic marker not only for fluorescence but also for optoacoustic techniques by virtue of its large absorption cross section and low quantum yield [144]. Another approach is synthesis of up-converting nanoparticles with the fluorescence spectrum shifted toward the short-wavelength region relative to the excitation spectrum. The use of such particles practically excludes the influence of autofluorescence background, limiting the sensitivity of fluorescence techniques during registration of emission.

One more important issue is the use of new spectral ranges, e.g., 1300–1700 nm, where the water absorption coefficient has local minima and scattering is much less pronounced than in the 700–900 nm range.

It is worthwhile to note that improvement of the elemental base of optical methods (creation of compact laser systems and high-frequency detectors, the use of fiberoptic technologies) along with accumulation of preclinical and clinical data promotes their increasingly wider application in medical diagnostics, despite the strong competition of traditional US, X-ray, and MRI techniques.

Analysis of the market of commercially available instruments for optical biomedical visualization shows that their application decreases with the size of study objects. In microscopy, practically any new technology, e.g., STORM, STED, selective plane illumination microscopy (SPIM), and ultramicroscopy, is very quickly introduced into industrial production by big companies such as Olympus, Zeiss, Nikon, and Leica. In contrast, commercial devices for fluorescence and optoacoustic visualization of laboratory animals are much fewer, probably because the market for them is small. Medical diagnostic tools (OCT, OA, fluorescence micro- and macroscopy) are even less popular, in the first place because it is very difficult to have them FDA-approved. Moreover, in general, clinicians are virtually unaware of new optical devices and their possible applications.

The present study was supported by the Russian Foundation for Basic Research (grant 13-04-40306-H). The author is grateful to N M Shakhova, P V Subochev, A G Orlova, and M Yu Kirillin for their valuable comments and discussions. Special thanks are due to G V Gelikonov, who provided STORM and OCT images of biological objects.

References

1. Tuchin V V (Ed.) *Handbook of Optical Biomedical Diagnostics* (Washington, DC: SPIE Press, 2002); *Opticheskaya Biomeditsinskaya Diagnostika* (Optical Biomedical Diagnostics) (Moscow: Fizmatlit, 2007)
2. Beard P *Interface Focus* **1** 602 (2011)
3. Nachabé R et al. *Biomed. Opt. Express* **2** 600 (2011)
4. Jacques S "Optical absorption of melanin" (accessed date: 12.01.2016), http://omlc.org/spectra/melanin/pheomelanin.html
5. Taroni P et al. *J. Biomed. Opt.* **12** 014021 (2007)
6. Nachabé R et al. *J. Biomed. Opt.* **16** 087010 (2011)
7. Ishimaru A *Wave Propagation and Scattering in Random Media* (New York: Academic Press, 1978); Translated into Russian: *Rasprostranenie i Rasseyanie Voln v Sluchaino-Neodnorodnykh Sredakh* (Moscow: Mir, 1981)
8. Gorshkov A V, Kirillin M Yu *J. Biomed. Opt.* **20** 085002 (2015)
9. Krafft C et al. *J. Biomed. Opt.* **17** 040801 (2012)
10. Tichauer K M et al. *Phys. Med. Biol.* **60** R239 (2015)
11. König K *J. Microsc.* **200** 83 (2000)
12. Ivanov A A, Alfimov M V, Zheltikov A M *Phys. Usp.* **47** 687 (2004); *Usp. Fiz. Nauk* **174** 743 (2004)
13. Uchugonova A et al. *Cell Cycle* **10** 2017 (2011)
14. Balu M et al. *JAMA Dermatology* **151** 1068 (2015)
15. Dimitrow E et al. *J. Invest. Dermatol.* **129** 1752 (2009)
16. Horton N G et al. *Nature Photon.* **7** 205 (2013)
17. Hell S, Stelzer E H K *Opt. Commun.* **93** 277 (1992)
18. Westphal V, Hell S W *Phys. Rev. Lett.* **94** 143903 (2005)
19. Rust M J, Bates M, Zhuang X *Nature Meth.* **3** 793 (2006)
20. van de Linde S et al. *Nature Protoc.* **6** 991 (2011)
21. Gustafsson M G L *Proc. Natl. Acad. Sci. USA* **102** 13081 (2005)
22. Yamanaka M, Smith N I, Fujita K *Microscopy* **63** 177 (2014)
23. Sharpe J et al. *Science* **296** 541 (2002)
24. Huisken J, Stainier D Y R *Development* **136** 1963 (2009)
25. Huisken J et al. *Science* **305** 1007 (2004)
26. Dodt H-U et al. *Nature Meth.* **4** 331 (2007)
27. Morozov A N et al. *Quantum Electron.* **40** 842 (2010); *Kvantovaya Elektron.* **40** 842 (2010)
28. Huang D et al. *Science* **254** 1178 (1991)
29. Sull A C et al. *Retina* **30** 235 (2010)
30. Regatieri C V et al. *Retina* **32** 563 (2012)
31. Mowatt G et al. *Health Technol. Assess.* **18** 1 (2014)
32. Vakoc B J et al. *Nature Rev. Cancer* **12** 363 (2012)
33. Mahmood U et al. *Am. J. Rhinol.* **20** 155 (2006)
34. Panteleeva O G et al. *Vestn. Rentgenolog. Radiolog.* (4) 50 (2012)
35. Davoudi B et al. *J. Biomed. Opt.* **18** 076008 (2013)
36. Gudmundsdottir I et al. *Open Heart* **2** e000225 (2015)
37. Dolin L S et al., in *Coherent-Domain Optical Methods. Biomedical Diagnostics, Environmental and Material Science* (Ed. V V Tuchin) (New York: Kluwer Acad. Publ., 2004) p. 211
38. Dolin L S *Phys. Usp.* **52** 519 (2009); *Usp. Fiz. Nauk* **179** 553 (2009)
39. Turchin I V et al. *J. Biomed. Opt.* **10** 064024 (2005)
40. Feldchtein F I et al. *Optics Express* **3** 257 (1998)
41. Sergeev A M et al. *Opt. Express* **1** 432 (1997)
42. Fujimoto J G et al. *Neoplasia* **2** 9 (2000)
43. Boppart S A et al. *Radiology* **208** 81 (1998)
44. Shakhov A V et al. *J. Surg. Oncol.* **77** 253 (2001)
45. Shakhova N M et al. *Laser Phys.* **12** 617 (2002)
46. De Boer J F et al. *IEEE J. Sel. Topics Quantum Electron.* **5** 1200 (1999)
47. Matveev L A et al. *Opt. Lett.* **40** 1472 (2015)
48. Briers J D, Webster S *J. Biomed. Opt.* **1** 174 (1996)
49. Vilenskii M A et al. *Quantum Electron.* **42** 489 (2012); *Kvantovaya Elektron.* **42** 489 (2012)
50. Robles F E et al. *Nature Photon.* **5** 744 (2011)
51. Izatt J A et al. *IEEE J. Sel. Topics Quantum Electron.* **2** 1017 (1996)
52. Gelikonov V M et al. *Radiophys. Quantum Electron.* **46** 550 (2003); *Izv. Vyssh. Uchebn. Zaved. Radiofiz.* **46** 610 (2003)
53. Dubois A, Moreau J, Boccara C *Opt. Express* **16** 17082 (2008)
54. Wang R K et al. *J. Opt. Soc. Am. B* **18** 948 (2001)
55. Genina E A, Bashkatov A N, Tuchin V V *Expert Rev. Med. Devices* **7** 825 (2010)
56. Sirotkina M A et al. *J. Nanopart. Res.* **13** 283 (2011)
57. Kirillin M Yu et al. *J. Biomed. Opt.* **14** 021017 (2009)
58. Thrane L et al. *Opt. Lett.* **29** 1641 (2004)
59. Kirillin M et al. *J. Biomed. Opt.* **17** 081413 (2012)
60. Esenaliev R O, Karabutov A A, Oraevsky A A *IEEE J. Sel. Topics Quantum Electron.* **5** 981 (1999)
61. Kruger R A et al. *Med. Phys.* **37** 6096 (2010)
62. Kim C, Favazza C, Wang L V *Chem. Rev.* **110** 2756 (2010)
63. Razansky D, Buehler A, Ntziachristos V *Nature Protoc.* **6** 1121 (2011)
64. Jathoul A P et al. *Nature Photon.* **9** 239 (2015)
65. Subochev P et al. *Laser Phys. Lett.* **13** 025605 (2016)
66. Rosenthal A, Ntziachristos V, Razansky D *Curr. Med. Imaging Rev.* **9** 318 (2013)
67. Perekatova V V, Fiks I I, Subochev P V *Radiophys. Quantum Electron.* **57** 67 (2014); *Izv. Vyssh. Uchebn. Zaved. Radiofiz.* **57** 75 (2014)
68. Neuschmelting V et al. *Photoacoustics* **4** 1 (2015)
69. Oraevsky A A, in *Biomedical Photonics Handbook* (Ed. T Vo-Dinh) (Boca Raton: CRC Press, Taylor and Francis Group, 2015) p. 715
70. Heijblom M et al. *Opt. Express* **20** 11582 (2012)
71. Taruttis A et al. *PLoS One* **7** e30491 (2012)
72. Yao J, Wang L V *Photoacoustics* **2** 87 (2014)
73. Subochev P et al. *Opt. Lett.* **37** 4606 (2012)
74. Subochev P et al. *Biomed. Opt. Express* **6** 631 (2015)
75. Wurzinger G et al. *Biomed. Opt. Express* **4** 1380 (2013)

76. Subochev P *Opt. Lett.* **41** 1006 (2016)
77. Yang J-M et al. *Nature Med.* **18** 1297 (2012)
78. Subochev P V et al. *Dokl. Phys.* **59** 59 (2014); *Dokl. Ross. Akad. Nauk* **454** 396 (2014)
79. Taruttis A, Ntziachristos V *Nature Photon.* **9** 219 (2015)
80. Menke J *Eur. Radiol.* **25** 2205 (2015)
81. Mallidi S et al. *Theranostics* **5** 289 (2015)
82. Zackrisson S, van de Ven S M, Gambhir S S *Cancer Res.* **74** 979 (2014)
83. Zhou Y et al. *J. Biophoton.* **8** 961 (2015)
84. Yao J, Wang L V *Neurophotonics* **1** 1877516 (2014)
85. Allen T J et al. *J. Biomed. Opt.* **17** 061209 (2012)
86. Hu Z et al. *Int. J. Ophthalmol. Eye Res.* **03** 126 (2015)
87. Tuchin V V *Phys. Usp.* **40** 495 (1997) ; *Usp. Fiz. Nauk* **167** 517 (1997)
88. Jacques S L *Phys. Med. Biol.* **58** R37 (2013)
89. Chung S H et al. *Phys. Med. Biol.* **53** 6713 (2008)
90. Shah N et al. *Disease Markers* **19** 95 (2004)
91. Tromberg B J et al. *Neoplasia* **2** 26 (2000)
92. Patterson M S, Chance B, Wilson B C *Appl. Opt.* **28** 2331 (1989)
93. Yodh A G, Boas D A, in *Biomedical Photonics Handbook* (Ed. T Vo-Dinh) (Boca Raton: CRC Press, 2003) Ch. 21
94. Bevilacqua F et al. *Appl. Opt.* **39** 6498 (2000)
95. Zimnyakov D A, Tuchin V V *Quantum Electron.* **32** 849 (2002); *Kvantovaya Elektron.* **32** 849 (2002)
96. Arridge S R *Inverse Probl.* **15** R41 (1999)
97. Konovalov A B et al. *Quantum Electron.* **36** 1048 (2006); *Kvantovaya Elektron.* **36** 1948 (2006)
98. Tret'yakov E V, Shuvalov V V, Shutov I V *Quantum Electron.* **32** 941 (2002); *Kvantovaya Elektron.* **32** 941 (2002); *Quantum Electron.* **31** 1095 (2001); *Kvantovaya Elektron.* **31** 1095 (2001)
99. Choe R et al. *J. Biomed. Opt.* **14** 024020 (2009)
100. Maslennikova A V et al. *J. Biophoton.* **3** 743 (2010)
101. Boas D A et al. *IEEE Signal Process. Mag.* **18** 57 (2001)
102. Gibson A P, Hebden J C, Arridge S R *Phys. Med. Biol.* **50** R1 (2005)
103. Durduran T et al. *Rep. Prog. Phys.* **73** 076701 (2010)
104. Eggebrecht A T et al. *NeuroImage* **61** 1120 (2012)
105. Carpenter C M et al. *Opt. Lett.* **32** 933 (2007)
106. Godavarty A et al. *Breast Cancer Targets Therapy* **7** 193 (2015)
107. Taroni P et al. *Phys. Med. Biol.* **50** 2469 (2005)
108. Orlova A G et al. *Laser Phys. Lett.* **5** 321 (2008)
109. Thomas D et al. *J. Biomed. Opt.* **17** 071311 (2012)
110. Ntziachristos V et al. *Nature Biotechnol.* **23** 313 (2005)
111. Pogue B W et al. *Technol. Cancer Res. Treat.* **3** 15 (2004)
112. Leblond F et al. *J. Photochem. Photobiol. B* **98** 77 (2010)
113. Themelis G et al. *J. Biomed. Opt.* **14** 064012 (2009)
114. Goriainov S A et al. *J. Neurosurgery* **78** (2) 21 (2014); *Vopr. Neirokhirurg.* **78** (2) 22 (2014)
115. Celli J P et al. *Chem. Rev.* **110** 2795 (2010)
116. Kleshnin M S et al. *Laser Phys. Lett.* **12** 115602 (2015)
117. Sheng C et al. *Photochem. Photobiol.* **8**3 738 (2007)
118. Fiks I *Int. J. Comput. Meth.* **11** 1350071 (2014)
119. Ntziachristos V, Weissleder R *Opt. Lett.* **26** 893 (2001)
120. Kleshnin M S, Turchin I V *Laser Phys. Lett.* **10** 075601 (2013)
121. Stuker F, Ripoll J, RudinM *Pharmaceutics* **3** 229 (2011)
122. Corlu A et al. *Opt. Express* **15** 6696 (2007)
123. Godavarty A et al. *Phys. Med. Biol.* **48** 1701(2003)
124. Deliolanis N C et al. *J. Biomed. Opt.* **13** 044008 (2008)
125. Darne C, Lu Y, Sevick-Muraca E M *Phys. Med. Biol.* **59** R1 (2014)
126. Chaudhari A J et al. *Med. Biol.* **54** 4687 (2009)
127. Freyer M et al. *J. Biomed. Opt.* **15** 036006 (2010)
128. Nahrendorf M et al. *Proc. Natl. Acad. Sci. USA* **107** 7910 (2010)
129. Kleshnin M et al. *Photon. Lasers Med.* **4** 85 (2015)
130. Sun Y, Day R N, Periasamy A *Nature Protoc.* **6** 1324 (2011)
131. Shcherbo D et al. *BMC Biotechnol.* **9** 24 (2009)
132. Nothdurft R E et al. *J. Biomed. Opt.* **14** 024004 (2009)
133. Rusanov A L et al. *J. Biophoton.* **3** 774 (2010)
134. McGinty J et al. *Biomed. Opt. Express* **2** 1907 (2011)
135. Filonov G S et al. *Nature Biotechnol.* **29** 757 (2011)
136. Tsoi K M et al. *Accounts Chem. Res.* **46** 662 (2013)
137. Xu C T et al. *Laser Photon. Rev.* **7** 663 (2013)
138. Khaydukov E V et al. *Biomed. Opt. Express* **5** 1952 (2014)
139. Nyk M et al. *Nano Lett.* **8** 3834 (2008)
140. Vinegoni C et al. *Opt. Lett.* **34** 2566 (2009)
141. Xu C T, Axelsson J, Andersson-Engels S *Appl. Phys. Lett.* **94** 251107 (2009)
142. Grebenik E A et al. *J. Biomed. Opt.* **18** 076004 (2013)
143. Hong G et al. *Nature Photon.* **8** 723 (2014)
144. Deliolanis N C et al. *Mol. Imag. Biol.* **16** 652 (2014)